USING GEOTAIL, WIND, AND POLAR OBSERVATIONS OF SOLAR, INTERPLANETARY, AND TERRESTRIAL PLASMA WAVE AND RADIO EMISSIONS TO IDENTIFY SOURCE CHARACTERISTICS

R. R. Anderson*, H. Matsumoto†, K. Hashimoto†,
H. Kojima†, I. Nagano‡, Y. Kasaba§,
M. L. Kaiser¶, J.-L. Bougeret‖, and J.-L. Steinberg‖

Abstract

GEOTAIL and POLAR Plasma Wave (PWI) and WIND Radio Science (WAVES) experiments' detections from typically widely separated positions of emissions are compared and contrasted in order to study the plasma characteristics near the sources and the generation mechanisms. Type III Solar radio bursts are detected at the onset of Solar flares. Observations of their generation at the fundamental and harmonics of the electron plasma frequency (f_{pe}) yield details of density and structure in the Solar corona and wind from within a few Solar radii to many AU beyond the Earth's orbit. Type II interplanetary kilometric Solar radio bursts are generated at interplanetary shocks driven ahead of ejecta from coronal mass ejections (CMEs) and allow the remote tracking of the CMEs. When the simultaneous observations of these radio bursts are not similar, one can often deduce high density regions blocking portions of the emissions. Electron plasma frequency, f_{pe}, emissions in the upstream Solar wind allow detection of abrupt density changes including those from Solar flare and CME driven interplanetary shocks. Comparisons of the remote $2f_{pe}$ emissions generated in the electron foreshock with in situ f_{pe} emissions as well as the comparison of in situ f_{pe} emissions between widely separated spacecraft identify temporal and spatial changes in the Solar wind density structure. Numerous terrestrial wave phenomena often begin or increase in intensity following the arrival

*The University of Iowa, Department of Physics and Astronomy, Iowa City, IA 52242, USA
†Radio Science Center for Space and Atmosphere, Kyoto University, Uji, Kyoto 611–0011, Japan
‡Department of Electrical and Computer Engineering, Faculty of Technology, Kanazawa University, 2–40–20, Kodatsuno, Kanazawa 920, Japan
§The Institute of Space and Astronautical Science, 3–1–1, Yoshinodai, Sagamihara, Kanagawa 229, Japan
¶NASA Goddard Space Flight Center, Greenbelt, MD 20771, USA
‖DESPA–URA CNRS 264, Observatoire de Paris–Meudon, F–91295 Meudon Cedex, France

at Earth of the plasma associated with the Solar radio bursts. These include auroral kilometric radiation (AKR), continuum storms, escaping terrestrial continuum radiation, and kilometric continuum. Increased AKR intensity and bandwidth are known to be related to increased geomagnetic activity and indicate enhanced energetic electron precipitation and expanding source regions. Comparison of the AKR observations from POLAR PWI in the auroral region, GEOTAIL PWI in the tail or Solar wind, and WIND WAVES in the Solar wind can help distinguish whether bandwidth differences are due to the sources or to propagation. Similarly, enhanced AKR and kilometric continuum can be distinguished from type II interplanetary kilometric Solar bursts when WIND is sufficiently far from GEOTAIL.

1 Introduction

Matsumoto et al. [1994, 1998] have described in detail the variety of plasma waves throughout Geospace and the Solar wind that are detected by the GEOTAIL Plasma Wave Instrument (PWI) since launch in July of 1992. The WIND Radio and Plasma Wave Investigation (WAVES) [Bougeret et al., 1995] was launched in November of 1994 and continues to provide high quality data today. The POLAR PWI [Gurnett et al., 1995] was launched in February 1996 and operated until mid–September 1997. Observations from these experiments both individually and collectively have offered many opportunities for investigating and determining the sources of many emissions.

Following the pioneering work of Steinberg et al. [1988, 1990, 1998] using ISEE 1 and 3, numerous studies have concentrated on terrestrial low frequency (LF) bursts using GEOTAIL, WIND, and/or POLAR [Kaiser et al., 1996a; Desch et al., 1996; Anderson et al., 1997, 1998; Desch, 1997; Desch and Farrell, 2000]. These studies have shown that LF bursts are the low frequency extension of terrestrial auroral kilometric radiation (AKR) and are well correlated with increased geomagnetic activity measured by a number of indices. Desch et al. [1996] used 1-hr averaged Solar wind data and found that the occurrence of LF bursts were well correlated with the Solar wind speed. For two of the most active periods in 1995, Desch [1997] performed a superposed epoch analysis of 92-s IMF data relative to the onset of LF bursts and found a pronounced negative bay in B_z approximately 40 minutes prior to the onsets. He concluded that the previous result might have been due to the fact that many more negative bays occur in faster Solar winds.

The characteristics of AKR have been well studied using individual spacecraft [e.g., Kaiser and Alexander, 1977a,b; Gurnett and Anderson, 1981; Kasaba et al., 1997b]. Comparison of the higher frequency components of AKR simultaneously observed by GEOTAIL and WIND has been carried out by Hashimoto et al. [1998a]. Several studies have shown the near simultaneous onset of AKR with earthward flow bursts in the inner magnetotail, auroral brightening, geosynchronous particle injections, and magnetic activity [e.g., Fairfield et al., 1999; Liou et al., 2000]. Hashimoto et al. [1998b] also have investigated the source of auroral myriametric radiation often detected with AKR and LF bursts. Escaping terrestrial continuum radiation [Kasaba et al., 1998] and kilometric continuum

[Hashimoto et al., 1999a,b] are frequently observed radiating out of the Earth's magnetosphere. These radiations are believed to be generated near the electron plasma frequency at steep density gradients near the plasmapause and inside the plasmasphere.

Leblanc et al. [1998] provides an excellent tutorial on determining the electron density from the Solar corona to the Earth's orbit using WAVES observations of type III Solar radio bursts. Reiner [2000] has shown how interplanetary type II Solar radio emissions associated with coronal mass ejections (CMEs) also help map out the electron density in the interplanetary medium. In situ measurements of the lower limit of the quasi–thermal noise line at the local electron plasma frequency, f_{pe}, provide the local electron density. Reiner et al. [1996, 1997] and Kasaba et al., [1997a, 2000] have shown that $2f_{pe}$ emissions are emitted from the Earth's electron foreshock region.

The following observations illustrate how the sources of the emissions discussed above can be studied using the GEOTAIL, WIND, and POLAR spacecraft and numerous ground sites.

2 Observations

The period from 13 UT to 23 UT on October 19, 1996, was particularly interesting for the variety of plasma wave emissions observed in the GEOTAIL PWI and WIND WAVES data. It was a geomagnetically disturbed period with K_p for the entire day being 4+, 4+, 4-, 5-, 5, 5+, 3+, and 5+. GEOTAIL was at apogee in the Solar wind near dawn about 30 R_E from the Earth. Figure 1 displays the two highest frequency bands of the GEOTAIL PWI Electric Sweep Frequency Analyzer (SFA) data over a 70 dB dynamic range. The SFA has five bands and the frequency steps within each band are linearly spaced [Matsumoto et al., 1994]. The top two bands cover 12.5 kHz to 100 kHz, and 100 kHz to 800 kHz.

WIND was in the Solar wind near 10 MLT (magnetic local time) (near morning) 131 R_E from the Earth. At 13 UT, GSE X = 110.1 R_E, GSE Y = -70.9 R_E, and GSE Z = -2.1 R_E and at 23 UT, GSE X = 111.3 R_E, GSE Y = -70.5 R_E, and GSE Z = -1.9 R_E. Figure 2 contains the WIND WAVES experiment's Thermal Noise Receiver (TNR) data for this time period. The TNR spectrogram is plotted on a linear frequency scale from 10 kHz to 256 kHz and covers a 20 dB dynamic range above background. Details of the WAVES experiment are found in Bougeret et al. [1995].

The two roughly horizontal narrow bands beginning near 20 kHz and 40 kHz in the GEOTAIL data and near 22 kHz and 40 kHz in the WIND data and ending near 18 kHz and 36 kHz in both figures are at the Solar wind f_{pe} and the second harmonic $2f_{pe}$ generated near the Earth's bow shock. f_{pe} equals 8.98 kHz times the square root of the number density N_e in electrons per cm^3. f_{pe} equaling 18 kHz, 20 kHz, 22 kHz, 36 kHz, and 40 kHz corresponds to N_e equaling 4.0 e-/cm^3, 5.0 e-/cm^3, 6.0 e-/cm^3, 16 e-/cm^3, and 20 e-/cm^3, respectively. The frequency spreading and intensity enhancements in the f_{pe} line in the GEOTAIL data are Langmuir waves (electron plasma oscillations) resulting from GEOTAIL being magnetically connected to the bow shock [Anderson et al., 1981;

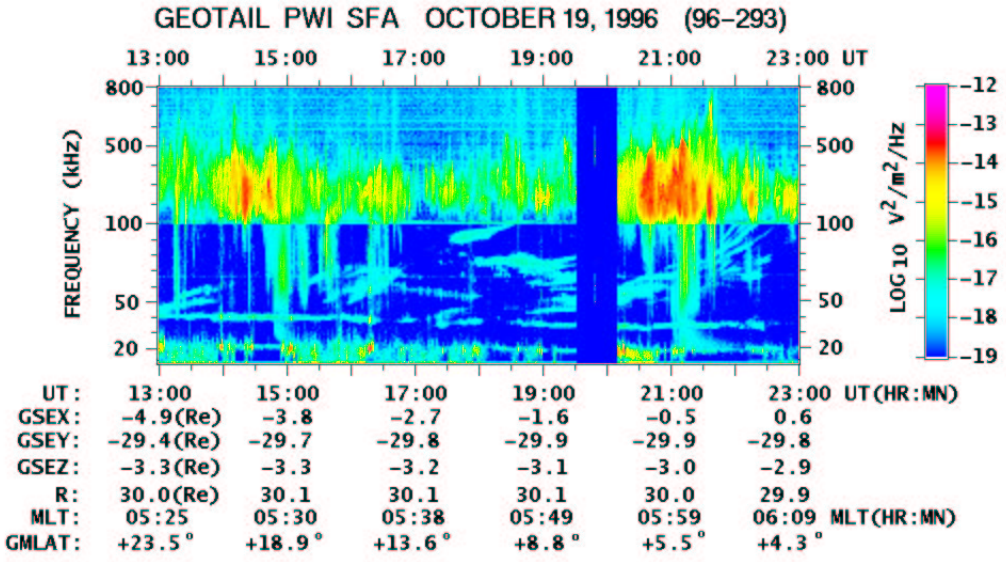

Figure 1: A spectrogram displaying the two highest frequency bands, 12.5 kHz to 100 kHz and 100 kHz to 800 kHz, of the GEOTAIL PWI Electric Sweep Frequency Analyzer (SFA) data from 13 UT to 23 UT on October 19, 1996. The plot covers a 70 dB dynamic range and the frequency steps within each band are linearly spaced. Selected orbit parameters are shown at the bottom of the plot below the time labels.

Kasaba et al., 2000]. The local f_{pe} is the lower limit of the quasi–thermal noise line (the lower band). Reiner et al. [1996, 1997] and Kasaba et al., [1997a, 2000] have shown that the $2f_{pe}$ emissions (the upper band) are emitted from the Earth's electron foreshock region along a line tangent to the contact point and correspond to the density at the bow shock. The $2f_{pe}$ emissions at both GEOTAIL and WIND closely follow two times the GEOTAIL f_{pe} emission because it is generated so much closer to Earth's bow shock.

Two LF bursts are evident between f_{pe} and $2f_{pe}$ just before 15 UT and just after 21 UT in both the GEOTAIL PWI and WIND WAVES data. Figure 3 shows the x–component magnetograms for 11 sites on the European International Monitor for Auroral Geomagnetic Effects (IMAGE) magnetometer network. The geographic and Pace [Baker and Wing, 1989] magnetic coordinates for the sites are listed in Table 1. The first LF burst corresponds to a strong narrow negative bay moving northward of 70° magnetic latitude and a positive spike moving southward. The negative bay at the Longyearbyen site (+75° magnetic latitude) goes below -1600 nT. The second LF burst corresponds to a disturbance that is broader but not quite as deep. Both LF bursts occurred during periods when the IMF B_z was negative. The Solar wind speed measured by the WIND Solar Wind Experiment (SWE) [Ogilvie et al., 1995] was near 600 km/s for the period. In the WIND WAVES data the diffuse falling tails of the LF bursts do not extend all the way down to the local f_{pe}. This implies that there is a region of slightly denser plasma between WIND and where the emission is scattered into the Solar wind. Note also that the second LF burst in the WAVES data has a tapered tail approaching about 22 kHz (6.0 e-/cm^3)

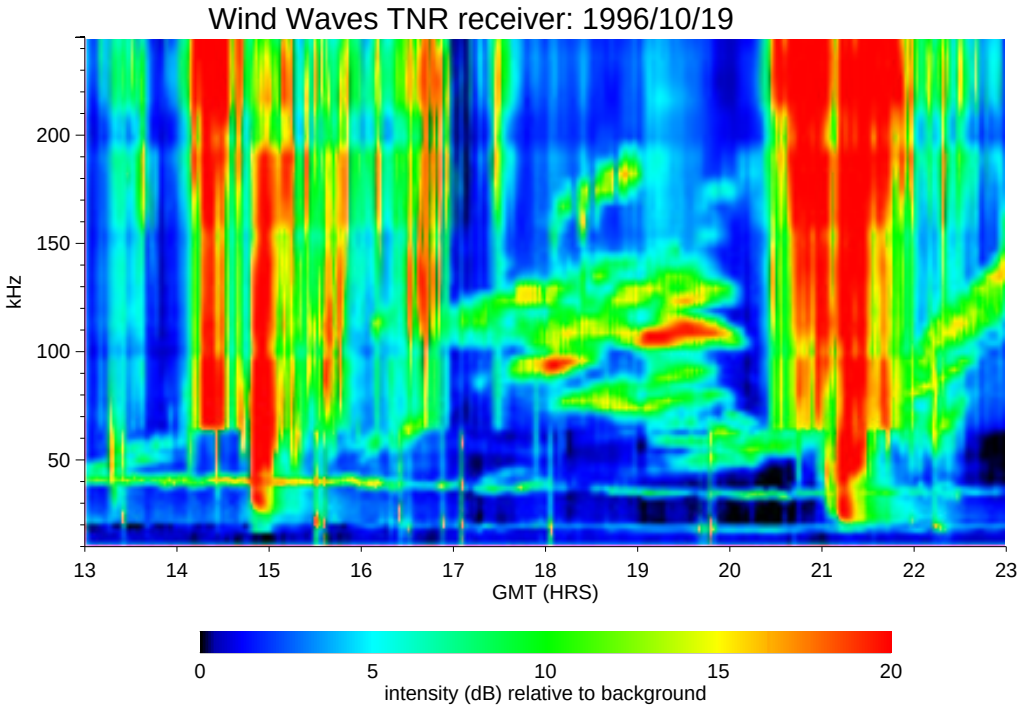

Figure 2: The WIND WAVES Thermal Noise Receiver (TNR) data for 13 UT to 23 UT on October 19, 1996. The spectrogram is plotted on a linear frequency scale from 10 kHz to 256 kHz and covers a 20 dB dynamic range above background.

Table 1: Image magnetometer network sites

Location	Code	Geographic		Pace Magnetic	
		Lat.	Long.	Lat.	Long.
Ny Alesund	NAL	78.92	11.95	75.99	112.89
Longyearbyen	LYR	78.20	15.82	74.92	113.90
Hornsund	HOR	77.00	15.60	73.93	110.98
Bear Island	BJN	74.50	19.20	71.25	109.33
Soroya	SOR	70.54	22.22	67.09	106.99
Masi	MAS	69.46	23.70	65.90	107.16
Muonio	MUO	68.02	23.53	64.43	105.90
Pello	PEL	66.90	24.08	63.25	105.53
Oulujarvi	OUJ	64.52	27.23	60.53	104.73
Hankasalmi	HAN	62.30	26.65	58.45	103.10
Nurmijarvi	NUR	60.50	24.65	56.90	100.65

while the local f_{pe} is about 18 kHz (4.0 e-/cm^3). The last time the density was that high was around 16 UT, six hours earlier. At 600 km/s, the Solar wind density would have convected about 2000 R_E downstream.

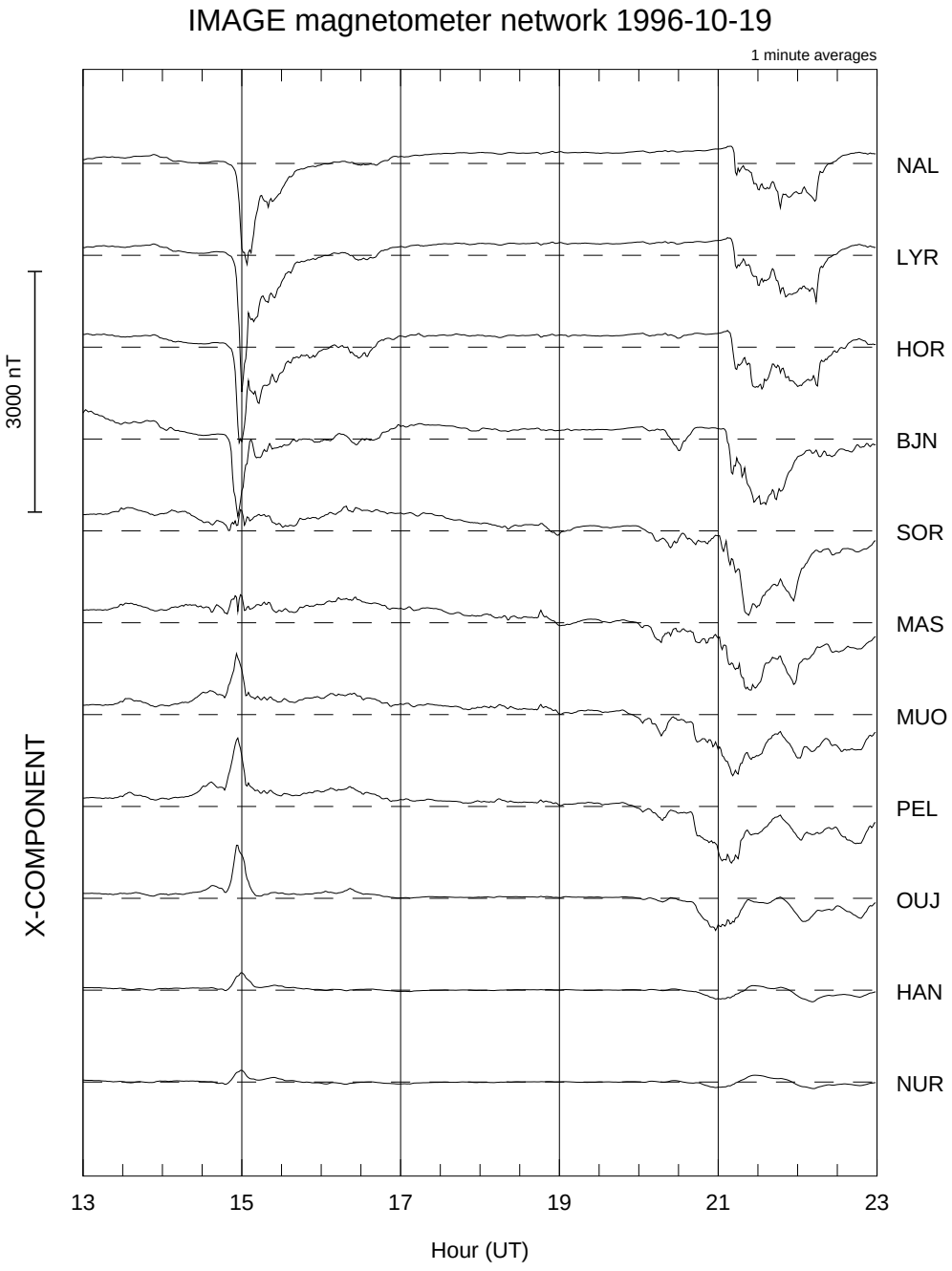

Figure 3: The north–south (X) component data for 11 sites on the IMAGE magnetometer network for 13 UT to 23 UT on October 19, 1996. The geographic and Pace magnetic coordinates for the sites are listed in Table 1. The scale is shown on the left and the vertical separation for the dashed lines for each panel are 1145 nT apart.

Two types of propagating electromagnetic emissions above $2f_{pe}$ to slightly above 100 kHz are evident in Figure 1. The nearly vertical emissions are low frequency continuations of the strong AKR found in the upper band. Note that the strongest AKR in the lower band is a part of the two LF bursts. Hashimoto et al., [1998b] refers to this as auroral myriametric radiation. The more nearly horizontal emissions with primarily positive slopes are escaping terrestrial continuum radiation [Kasaba et al., 1998] that evolves at higher frequencies into kilometric continuum [Hashimoto et al., 1999a,b]. These radiations are believed to be generated near the electron plasma frequency at steep density gradients near the plasmapause and inside the plasmasphere. The emissions often have multiple lines with a fixed or only slowly varying separation. The separation of the lines most likely indicates the local electron cyclotron frequency, f_{ce}, where the emissions are generated. High frequency resolution data from other spacecraft have shown that the n+1/2 f_{ce} or electron cyclotron harmonic, ECH, emissions near f_{pe} are enhanced especially near the geomagnetic equator. The free energy source is generally believed to be injected electrons from the plasma sheet drifting around the magnetosphere into the plasmasphere. The emissions near and above 100 kHz starting prior to 17 UT on WIND in Figure 2 are not detected in Figure 1 until after 18:30 UT, precisely when GEOTAIL dropped below 10° geomagnetic latitude. WIND on the other hand began near 12° geomagnetic latitude at 13 UT and dropped below 10° geomagnetic latitude at 17 UT. Hashimoto et al. [1999a,b] found that kilometric continuum in the 100–800 kHz range was tightly confined to ±10° geomagnetic latitude. These observations are in strong agreement.

AKR dominates the upper band in the GEOTAIL electric SFA data in Figure 1. It is especially enhanced in intensity at the times of the geomagnetic disturbances shown in Figure 3. This is also evident in the WIND WAVES RAD1 data shown in Figure 4. The spectrogram is linear in frequency from 20 kHz to 1040 kHz and covers a 20 dB dynamic range above background. Figure 5 is a plot of the electric field data from the POLAR PWI Sweep Frequency Receiver [Gurnett et al., 1995] for 13 UT to 23 UT on October 19, 1996, as POLAR moved in MLT from midnight to morning near its 9 R_E apogee at high latitudes. The spectrogram is linear in frequency from 10 kHz to 800 kHz, and has a 50 dB dynamic range. AKR is the dominate emission and its variable and bursty nature is quite evident. The strong enhancement of AKR around 14 UT when POLAR was near local midnight corresponds well with the first strong geomagnetic disturbance shown in Figure 3 and includes the first LF burst. When POLAR is high over the polar regions and especially when it is within about six hours of local midnight, it provides excellent observations of the majority of the AKR spectrum at its origin. The expanded AKR bandwidths and decreasing low frequency cutoff with increased geomagnetic activity were first observed by Kaiser and Alexander [1977a,b]. Since AKR is generated near the local electron cyclotron frequency, the lower the AKR frequency, the higher the altitude where it is generated and vice versa. AKR at 600 kHz is generated near a geocentric radial distance of 1.4 R_E in the auroral region, 400 kHz near 1.6 R_E, 200 kHz near 2.0 R_E, 100 kHz near 2.5 R_E and 30 kHz near 3.7 R_E [Gurnett and Anderson, 1981]. The LF bursts occurred near the middle of AKR events where the lower cutoff frequencies were the lowest.

When the intensities are normalized to a common radial distance, the remaining differences between the GEOTAIL, POLAR, and WIND AKR observations are primarily due

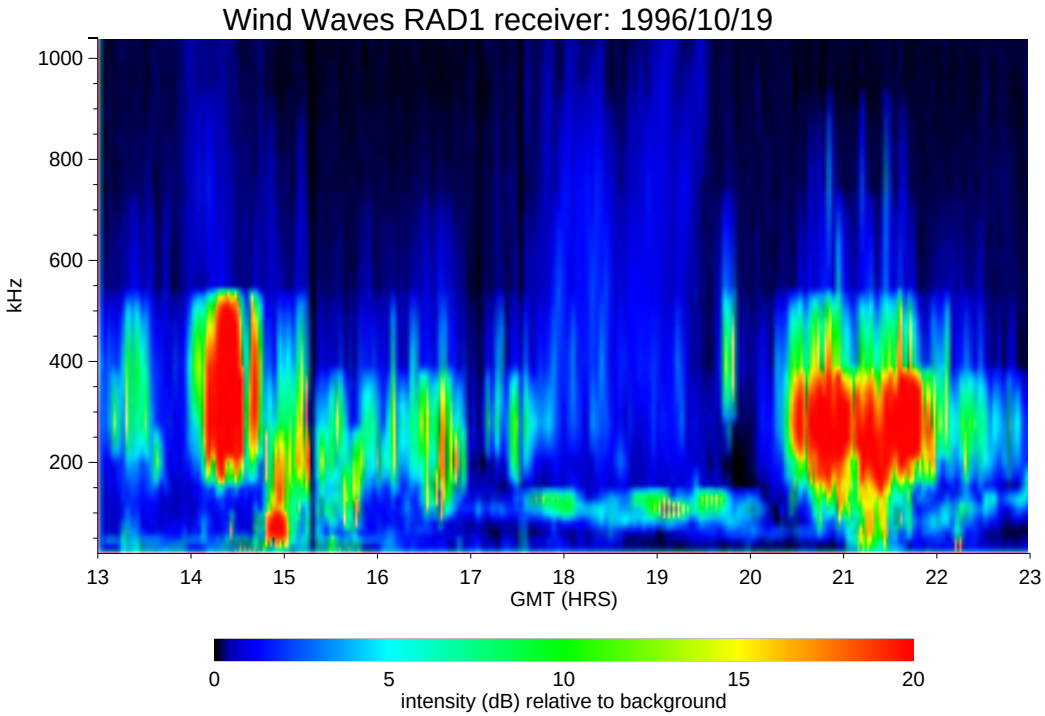

Figure 4: The WIND WAVES RAD1 data for 13 UT to 23 UT on October 19, 1996. The spectrogram is linear in frequency from 20 kHz to 1040 kHz and covers a 20 dB dynamic range above background.

to the differences in MLT of the spacecraft and the affect of the Earth's plasmasphere, magnetosphere, and magnetosheath on the propagation path [Hashimoto et al., 1998a]. For example, the AKR is much stronger at POLAR for the first LF burst event when POLAR was near local midnight. For the second LF burst, the AKR is more intense in the GEOTAIL data acquired near dawn than in the POLAR data from later in the morning. The AKR observed nearly continuously from 18 UT to 20 UT in the POLAR and GEOTAIL data is almost totally absent in the WIND data. The MLT at WIND was one to five hours later than at POLAR and four hours later than at GEOTAIL. This suggests that in order to not be detected at WIND, the source region was prior to local midnight. The relatively narrow band of emissions from about 40 kHz to 150 kHz in the WAVES RAD1 data is the escaping terrestrial continuum radiation and kilometric continuum also observed in the GEOTAIL PWI and WAVES TNR data.

Another period with interesting plasma wave emissions was 12 UT on November 18, 2000, to 12 UT on November 19, 2000. It was geomagnetically quieter than the October 19, 1996, period just discussed with K_p being 0, 0, 0, 0+, 1+, 1+, 3-, and 3 for November 18 and 2-, 2+, 2, 2, 1+, 2-, 1, and 2 for November 19. Figure 6 is a 24-hour spectrogram displaying the data from all three WIND WAVES receivers, TNR, RAD1, and RAD2, over a 20 dB dynamic range. The frequency scale is logarithmic from 4 kHz to 14 MHz. WIND was in the Solar wind near noon MLT 98 R_E from the Earth. At 12 UT on November 18, GSE X = 97.2 R_E, GSE Y = 7.5 R_E, GSE Z = 5.0 R_E, and MLT = 12:21. At 12 UT on

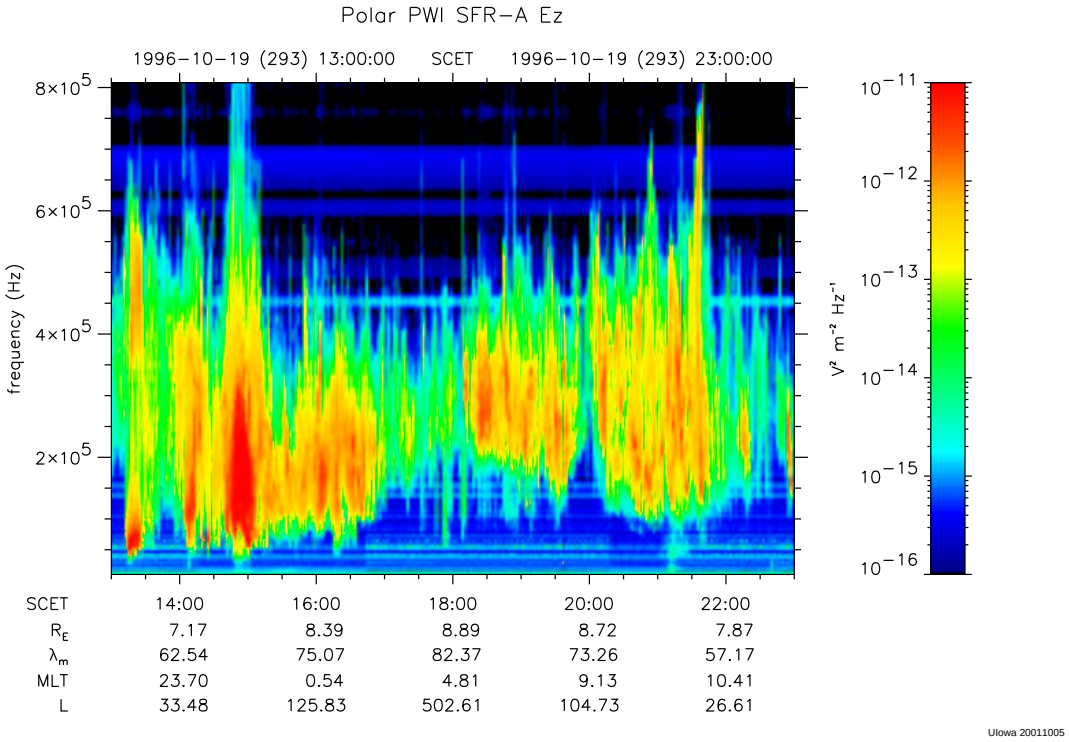

Figure 5: The electric field data from the POLAR PWI Sweep Frequency Receiver for 13 UT to 23 UT on October 19, 1996. The spectrogram is linear in frequency from 10 kHz to 800 kHz, and has a 50 dB dynamic range. Selected orbit parameters are shown at the bottom of the plot below the time labels.

November 19, GSE X = 96.3 R_E, GSE Y = 9.9 R_E, GSE Z = 4.4 R_E, and MLT = 12:49. The geomagnetic latitude was -14.15° at 12 UT on November 18, reached a maximum of -7.31° at 17 UT, reached a minimum of -29.37° at 05:24 UT on November 19, and rose to -17.25° at 12 UT. The two emission lines in the lower portion of the plot are the f_{pe} and $2f_{pe}$ lines. The primary emissions in the upper portion of the plot are type II and type III Solar radio bursts. The first full type III Solar radio burst was first detected at 14 MHz at 13:15 UT. The Solar flare that generated this burst was simultaneous with a CME believed to be the source of the type II interplanetary kilometric Solar radio bursts observed from 20 UT to 05 UT the next day with the fundamental frequency ranging from about 600 kHz down to 200 kHz. The type II bursts are generated at the first and second harmonics of the local f_{pe} at the interplanetary shock front pushed ahead of the CME [Cane et al., 1987]. Here the fundamental emission is the strongest but the second harmonic is still apparent. There are multiple elements and the frequency jumps several times. Direction finding yet to be done can distinguish whether the shock front has encountered a more dense plasma (the source direction remains the same) or whether the location of the source on the shock front has changed (the source direction changes). The estimated shock speed based on the frequency drift rate of the type II emission and a model of the number density distribution in the Solar wind [Reiner, 2000] is 450 km/s.

The GEOTAIL electric field data for the same time period are shown in Figure 7. The

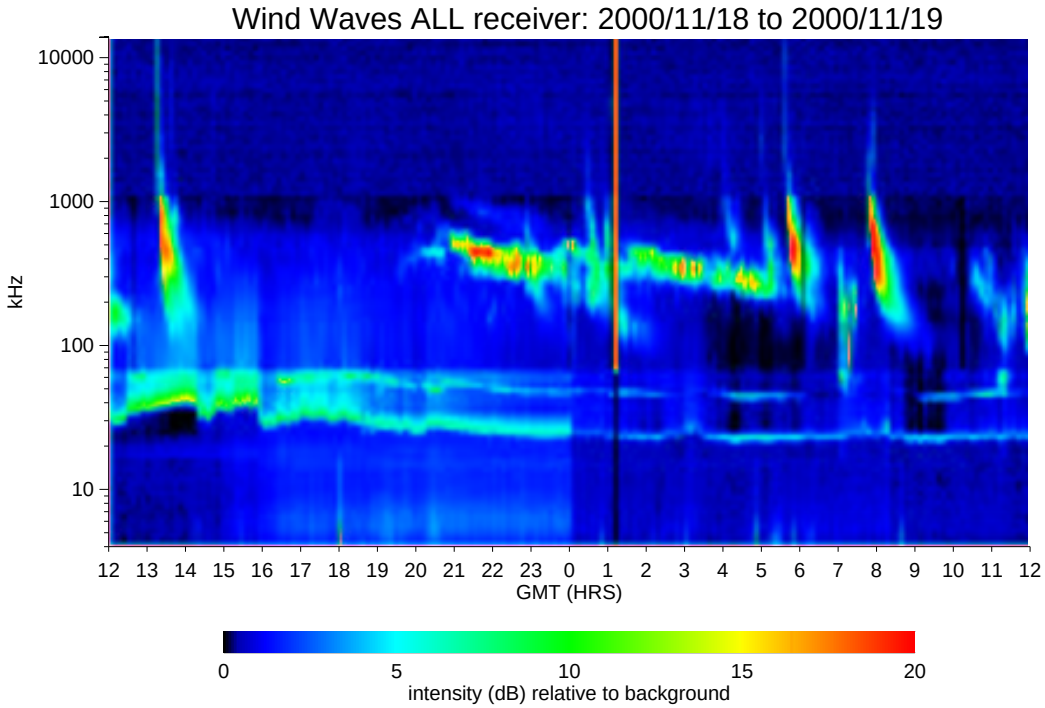

Figure 6: A spectrogram of the data from all three WIND WAVES receivers, TNR, RAD1, and RAD2, from 12 UT on November 18, 2000, to 12 UT on November 19, 2000. The plot covers a 20 dB dynamic range and the frequency scale is logarithmic from 4 kHz to 14 MHz.

plot is linear in frequency from 0 to 800 kHz and has a 30 dB dynamic range. GEOTAIL was near apogee in the morning Solar wind from 7 MLT to 9 MLT. The type III and type II Solar radio bursts detected by WIND WAVES are also detected by GEOTAIL. Spectral differences between the GEOTAIL and WIND observations of these phenomena as well as direction finding can be used to deduce density structures in the Solar wind. Two types of other plasma wave phenomena are detected in the GEOTAIL data that are not apparent in the WIND data. From 20 UT on November 18 to 01 UT on November 19, GEOTAIL PWI detected AKR (the nearly vertical structure) from about 100 kHz to almost 300 kHz and kilometric continuum radiation (the nearly horizontal structure) from about 100 kHz to 600 kHz. Figure 8 shows the x–component magnetograms for 10 sites on the IMAGE magnetometer network. A strong geomagnetic disturbance north of 60° magnetic latitude began around 20 UT and continued until 02 UT the next day in the vicinity of 65° magnetic latitude. On–line auroral imaging data from the POLAR VIS [Frank et al., 1995] were available from 19:06 UT to 20:17 UT. These data showed a compact auroral brightening near local midnight beginning around 19:14 UT north of Russia that expanded both in latitude and longitude and reached to northern Scandinavia by the time the data ended.

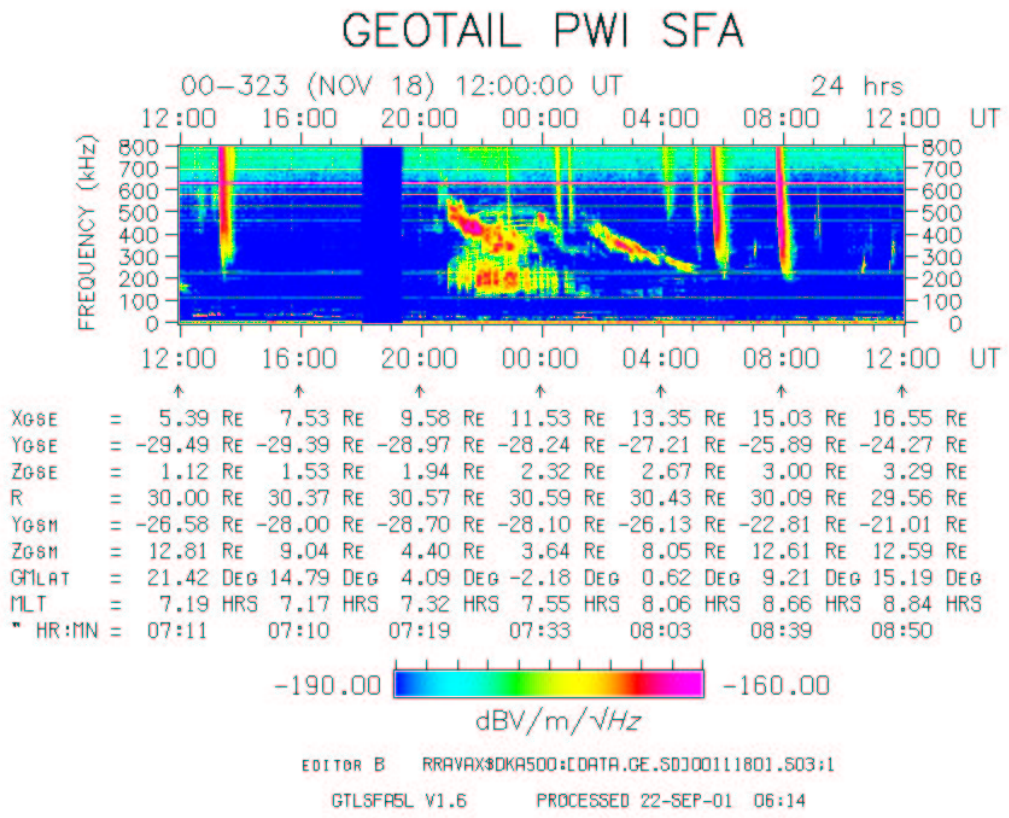

Figure 7: The GEOTAIL PWI electric field data for 12 UT on November 18, 2000, to 12 UT on November 19, 2000. The plot is linear in frequency from 0 to 800 kHz and has a 30 dB dynamic range. Selected orbit parameters are shown at the bottom of the plot below the time labels.

3 Discussion

In situ and remote plasma wave observations were able to show that there were differences in density between WIND and GEOTAIL during the October 19, 1996, event when the spacecraft were about 100 R_E apart in the morning Solar wind. At 13 UT f_{pe} at GEOTAIL was 20 kHz (5.0 e-/cm^3) while at WIND it was 22 kHz (6.0 e-/cm^3). In the WIND WAVES data the diffuse falling tail of the LF bursts do not extend all the way down to the local f_{pe}. When LF bursts have a lower cutoff frequency above the local f_{pe}, the implication is that there is a region of slightly denser plasma between WIND and where the emission is scattered into the Solar wind. Note also that the second LF burst in the WAVES data has a tapered tail approaching about 22 kHz (6.0 e-/cm^3) while the local f_{pe} is about 18 kHz (4.0 e-/cm^3). The last time the density was that high was around 16 UT, six hours earlier. At 600 km/s, the Solar wind density would have convected about 2000 R_E downstream. The LF bursts are believed to be due to low frequency AKR generated in the auroral regions propagating down the tail until the local f_{pe} in the magnetosheath and across the tail approaches the Solar wind f_{pe}. The waves are then scattered into the Solar wind where they can now be detected by spacecraft in the Solar wind. Prior

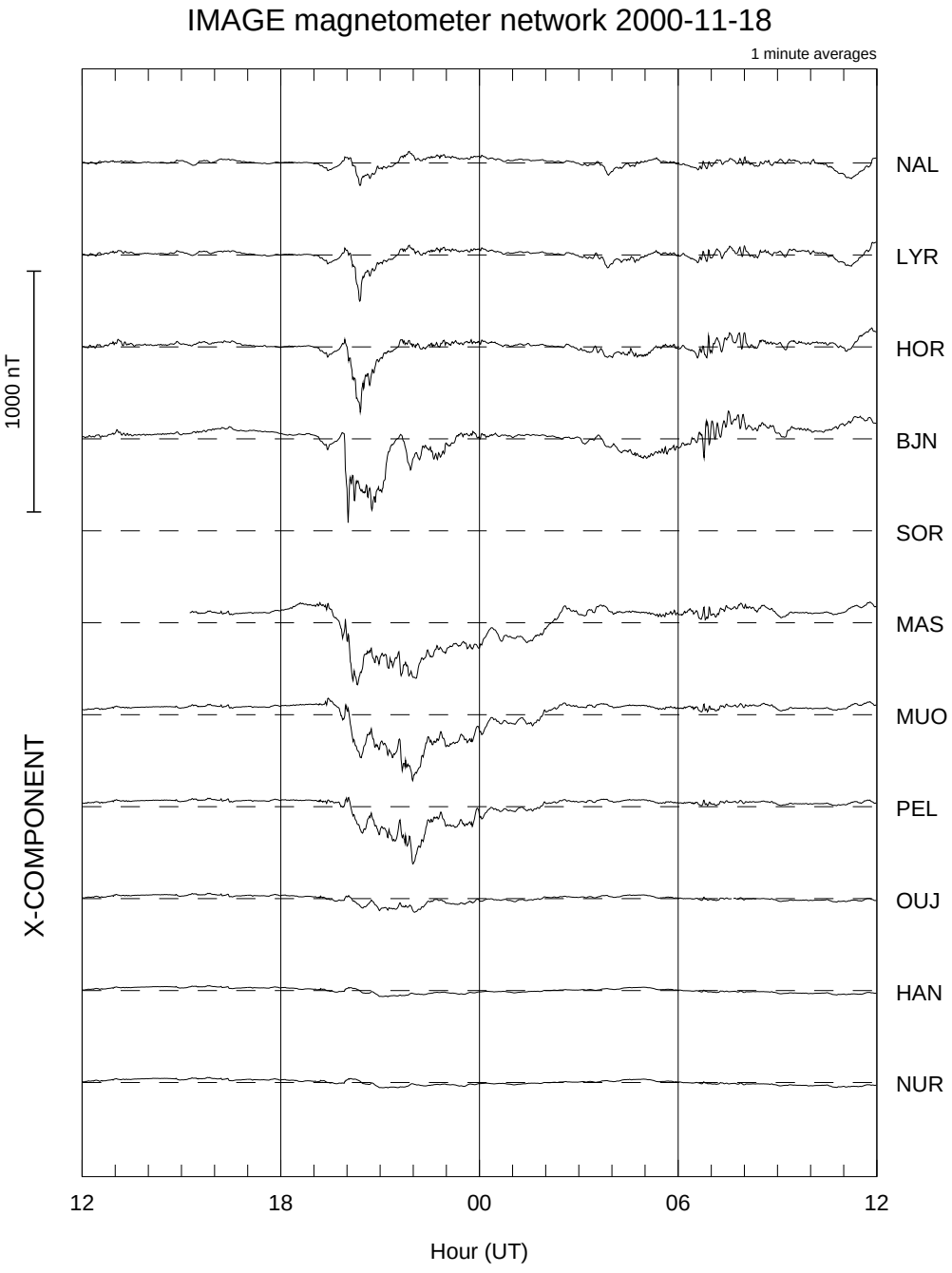

Figure 8: The north–south (X) component data for 10 sites on the IMAGE magnetometer network for 12 UT on November 18, 2000, to 12 UT on November 19, 2000. The scale is shown on the left and the vertical separation for the dashed lines for each panel are 380 nT apart.

to reaching that point, the higher f_{pe} in the magnetosheath blocked the emissions from reaching spacecraft upstream of that point. The frequency the tapered tail approaches is the local f_{pe} where the waves are scattered into the Solar wind. The distance down the tail where this occurs is estimated to be from greater than a hundred R_E [Desch, 1997] to around 2000 R_E or more [Steinberg et al., 1988, 1990] or somewhere in between [Steinberg et al., 1998; Desch and Farrell, 2000]. Our determination of 2000 R_E downstream is thus not unreasonable.

Spectral differences between the GEOTAIL and WIND observations of the type III and type II Solar radio bursts detected on November 18 and 19, 2000, by WIND WAVES and GEOTAIL as well as direction finding can be used to deduce density structures in the Solar wind. The type II Solar interplanetary kilometric radio bursts shown contain multiple elements and the frequency jumps several times. Direction finding yet to be done for this event can distinguish whether the shock front has encountered a more dense plasma (the source direction remains the same) or whether the location of the source on the shock front has changed (the source direction changes).

Careful inspection of the f_{pe} and $2f_{pe}$ lines in the WAVES data in Figure 6 shows that there is a modest jump in the local f_{pe} at 20:13 UT and in $2f_{pe}$ at 20:39. The Solar wind speed was about 370 km/s according to the SWE Key Parameter data. In 26 minutes this speed Solar wind would convect 90 R_E downstream, in very good agreement with the expected distance from WIND to the nose of the bow shock. The resultant pressure pulse, with a reasonable 20-minute delay to propagate through the magnetosheath to the tail, along with the negative Solar wind B_z might be the trigger pulse for the observed AKR intensification beginning around 21 UT. A longer delay through the magnetosheath and tail could account for the greater intensification beginning around 21:50 UT. The geomagnetic disturbances detected in the IMAGE magnetometer data began around 20 UT. The IMF B_z turned strongly southward around 19 UT at WIND and about 19:30 UT at GEOTAIL. A possible reason for the delayed AKR enhancement observation at GEOTAIL was that GEOTAIL was near 7 MLT and the AKR might have started sufficiently earlier than local midnight such that it could not be detected until the AKR source region had spread. The lack of detection of AKR at WIND was most likely due to its noon MLT location from which the Earth would totally block the source region and somewhat less to the significantly greater distance from the source region.

The nearly simultaneous observation of the kilometric continuum radiation with the AKR in the GEOTAIL may demonstrate a relationship or may be a pure coincidence. As noted earlier, Hashimoto et al. [1999a,b] found that kilometric continuum in the 100–800 kHz range was tightly confined to ±10° geomagnetic latitude. From 20 UT on November 18 to 01 UT on November 19, GEOTAIL's geomagnetic latitude ranged from +4.04° to -2.41°, always remaining very close to the magnetic equator. On the other hand, WIND's geomagnetic latitude ranged from -10.42° to -23.12° for the same period.

4 Summary

This study shows the high value of using multiple spacecraft and ground observations to investigate the inhomogeneous nature of space and the sources of the detected emissions. When in the Solar wind, both WIND and GEOTAIL provide detailed electron number density measurements in situ from detection of the f_{pe} line and at the bow shock from the $2f_{pe}$ observations. Remote observations, including direction finding and triangulation, of type III and type II kilometric interplanetary Solar radio bursts enable us to determine the spatial structure of the Solar wind.

We have confirmed that LF bursts are strongly correlated with strong and isolated geomagnetic disturbances and enhanced AKR. This report and previous LF burst studies suggest several topics to be further investigated. For example, "What are the characteristics of geomagnetic disturbances that result in LF bursts being observed and are there thresholds?" and "How does the magnetosheath density evolve as one moves down the geomagnetic tail?".

Continued research on AKR will help determine the relative importance of various storm and substorm triggering phenomena. Much remains to be learned about kilometric continuum radiation including the power source and the relationship to geomagnetic disturbances. The GEOTAIL PWI and WIND WAVES experiments continue to provide valuable data for collaboration with the more recent IMAGE and CLUSTER II missions.

Acknowledgements: We are grateful for the WIND SWE Key Parameter data provided through the courtesy of SWE PI Keith Ogilvie from GSFC and Alan Lazarus from MIT and John Steinberg from LANL who developed and certified the SWE KP data, for the OMNI data from the National Space Science Data Center courtesy of Joe King and Jim Green, and for the IMAGE magnetometer data from the WWW site http://www.geo.fmi.fi/image/index/html. The research at The University of Iowa was supported by NASA Grants NAG5–7710, NAG5–7943, NAG5–6127, and NAG5–6369, all with Goddard Space Flight Center.

References

Anderson, R. R., G. K. Parks, T. E. Eastman, D. A. Gurnett, and L. A. Frank, Plasma waves associated with energetic particles streaming into the Solar wind from the Earth's bow shock, *J. Geophys. Res.*, **86**, 4493, 1981.

Anderson, R. R., D. A. Gurnett, H. Matsumoto, K. Hashimoto, H. Kojima, Y. Kasaba, M. L. Kaiser, G. Rostoker, J.–L. Bougeret, J.–L. Steinberg, I. Nagano, and H. Singer, Observations of low frequency terrestrial type III bursts by GEOTAIL and WIND and their association with isolated geomagnetic disturbances detected by ground and space–borne instruments, in *Planetary Radio Emissions IV*, edited by H. O. Rucker, S. J. Bauer, and A. Lecacheux, Austrian Academy of Sciences Press, Vienna, 241–250, 1997.

Anderson, R. R., D. A. Gurnett, L. A. Frank, J. B. Sigwarth, H. Matsumoto, K. Hashimoto, H. Kojima, Y. Kasaba, M. L. Kaiser, G. Rostoker, J.–L. Bougeret, J.–L. Steinberg, I. Nagano, T. Murata, H. J. Singer, T. G. Onsager, and M. F. Thomsen, Geotail, Polar, Wind, CANOPUS, and ISTP associated geosynchronous satellite observations of plasma wave emissions and related magnetospheric phenomena during substorms, in *Proceedings of International Conf. on Substorms–4, ISC–4*, edited by S. Kokubun and Y. Kamide, 567–572, Kluwer Academic Publishers, 1998.

Baker, K. B., and S. Wing, A new magnetic coordinate system for conjugate studies at high latitudes, *J. Geophys. Res.*, **94**, 9139–9143, 1989.

Bougeret, J.–L., M. L. Kaiser, P. J. Kellogg, R. Manning, K. Goetz, S. J. Monson, N. Monge, L. Friel, C. A. Meetre, C. Perche, L. Sitruk, and S. Hoang, WAVES: The radio and plasma wave investigation on the WIND spacecraft, *Space Sci. Rev.*, **71**, 231–263, 1995.

Cane, H. V., N. R. Sheely Jr., and R. A. Howard, Energetic interplanetary shocks, radio emission, and coronal mass ejections, *J. Geophys. Res.*, **92**, 9869–9874, 1987.

Desch, M. D., M. L. Kaiser, and W. M. Farrell, Control of terrestrial low frequency bursts by Solar wind speed, *Geophys. Res. Lett.*, **23**, 1251–1254, 1996.

Desch, M. D., Terrestrial LF Bursts: Source and Solar wind connection, in *Planetary Radio Emissions IV*, edited by H. O. Rucker, S. J. Bauer, and A. Lecacheux, Austrian Academy of Sciences Press, Vienna, 251–258, 1997.

Desch, M. D., and W. M. Farrell, Terrestrial LF Bursts: Escape paths and wave intensification, *Radio Astronomy at Long Wavelengths in AGU Geophysical Monograph 119*, edited by R. G. Stone, K. W. Weiler, M. L. Goldstein, and J.–L. Bougeret, 205–211, 2000.

Fairfield, D. H., T. Mukai, M. Brittnacher, G. D. Reeves, S. Kokubun, G. K. Parks, T. Nagai, H. Matsumoto, K. Hashimoto, D. A. Gurnett, and T. Yamamoto, Earthward flow bursts in the inner magnetotail and their relation to auroral brightening, AKR intensifications, geosynchronous particle injections and magnetic activity, *J. Geophys. Res.*, **104**, 355–370, 1999.

Frank, L. A., J. B. Sigwarth, J. D. Craven, J. P. Cravens, J. S. Dolan, M. R. Dvorsky, P. K. Hardebeck, J. D. Harvey, and D. Muller, The Visible Imaging System (VIS) for the POLAR Spacecraft, *Space Sci. Rev.*, **71**, 297–328, 1995.

Gurnett, D. A., and R. R. Anderson, The kilometric radio emission spectrum: Relationship to auroral acceleration processes, *Physics of Auroral Arc Formation in Geophysical Monograph Series*, **25**, edited by S.–I. Akasofu and J. R. Kan, American Geophysical Union, 341–350, 1981.

Gurnett, D. A., A. M. Persoon, R. F. Randall, D. L. Odem, S. L. Remington, T. F. Averkamp, M. M. DeBower, G. B. Hospodarsky, R. L. Huff, D. L. Kirchner, M. A. Mitchell, B. T. Pham, J. R. Phillips, W. J. Schintler, P. Sheyko, and D. R. Tomash, The POLAR plasma wave instrument, *Space Sci. Rev.*, **71**, 597–622, 1995.

Hashimoto, K., H. Matsumoto, T. Murata, M. L. Kaiser, and J.–L. Bougeret, Comparison of AKR simultaneously observed by the GEOTAIL and WIND spacecraft, *Geophys. Res. Lett.*, **25**, 853–856, 1998a.

Hashimoto, K., S. Kudo, and H. Matsumoto, Source of auroral myriametric radiation observed with GEOTAIL, *J. Geophys. Res.*, **103**, 23475–23483, 1998b.

Hashimoto, K., W. Calvert, and H. Matsumoto, Kilometric continuum observed with Geotail, *Adv. Space Res.*, **24**, 63–66, 1999a.

Hashimoto, K., W. Calvert and H. Matsumoto, Kilometric continuum detected by Geotail, *J. Geophys. Res.*, **104**, 28645–28656, 1999b.

Kaiser, M. L., and J. K. Alexander, Terrestrial kilometric radiation 3. Average spectral properties, *J. Geophys. Res.*, **82**, 3273–3280, 1977a.

Kaiser, M. L., and J. K. Alexander, Relationship between auroral substorms and the occurrence of terrestrial kilometric radiation, *J. Geophys. Res.*, **82**, 5283–5286, 1977b.

Kaiser, M. L., M. D. Desch, W. M. Farrell, J.–L. Steinberg, and M. J. Reiner, LF band terrestrial radio bursts observed by Wind/WAVES, *Geophys. Res. Lett.*, **23**, 1283–1286, 1996a.

Kasaba, Y., H. Matsumoto, and R. R. Anderson, Geotail observation of $2f_p$ emission around the terrestrial electron foreshock, *Adv. Space Res.*, **20**, 699–702, 1997a.

Kasaba, Y., H. Matsumoto, K. Hashimoto, and R. R. Anderson, The angular distribution of auroral kilometric radiation observed by the GEOTAIL spacecraft., *Geophys. Res. Lett.*, **24**, 2483–2486, 1997b.

Kasaba, Y., H. Matsumoto, K. Hashimoto, R. R. Anderson, J.–L. Bougeret, M. L. Kaiser, X. Y. Wu, and I. Nagano, Remote sensing of the plasmapause during substorms: GEOTAIL observation of non–thermal continuum enhancement, *J. Geophys. Res.*, **103**, 20389–20405, 1998.

Kasaba, Y., H. Matsumoto, Y. Omura, R. R. Anderson, T. Mukai, Y. Saito, T. Yamamoto, and S. Kokubun, Statistical studies of plasma waves and backstreaming electrons in the terrestrial electron foreshock observed by Geotail, *J. Geophys. Res.*, **105**, 79–103, 2000.

Leblanc, Y., G. A. Dulk, and J.–L. Bougeret, Tracing the electron density from the corona to 1 AU, *Solar Phys.*, **183**, 165–180, 1998.

Liou, K., C.–I. Meng, A. T. Y. Lui, P. T. Newell, and R. R. Anderson, Auroral kilometric radiation at substorm onset, *J. Geophys. Res.*, **105**, 25325–25331, 2000.

Matsumoto, H., I. Nagano, R. R. Anderson, H. Kojima, K. Hashimoto, M. Tsutsui, T. Okada, I. Kimura, Y. Omura, and M. Okada, Plasma wave observations with GEOTAIL Spacecraft, *J. Geomag. Geoelectr.*, **46**, 59–95, 1994.

Matsumoto, H., H. Kojima, Y. Omura, and I. Nagano, Plasma waves in Geospace: GEOTAIL Observation, *New Perspectives on the Earth's Magnetotail in Geophysical*

Monograph 105, edited by N. Nishida, D. N. Baker, and W. H. Cowley, American Geophysical Union, 259–319, 1998.

Ogilvie, K. W., D. J. Chornay, R. J. Fitzenreiter, F. Hunsaker, J. Keller, J. Lobell, G. Miller, J. D. Scudder, E. C. Sittler, Jr., R. B. Torbert, D. Bodet, G. Needell, A. J. Lazarus, J. T. Steinberg, J. H. Tappan, A. Mavretic, and E. Gergin, SWE, A comprehensive plasma instrument for the WIND spacecraft, *Space Sci. Rev.*, **71**, 55–77, 1995.

Reiner, M. J., M. L. Kaiser, J. Fainberg, M. D. Desch, and R. G. Stone, $2f_p$ radio emissions from the vicinity of the Earth's foreshock: WIND observations, *Geophys. Res. Lett.*, **23**, 1247–1250, 1996.

Reiner, M. J., Y. Kasaba, M. L. Kaiser, H. Matsumoto, I. Nagano, and J.–L. Bougeret, $2f_p$ radio source location determined from WIND/GEOTAIL triangulation, *Geophys. Res. Lett.*, **24**, 919–922, 1997.

Reiner, M. J., Interplanetary type II radio emissions associated with CMEs, *Radio Astronomy at Long Wavelengths in AGU Geophysical Monograph 119*, edited by R. G. Stone, K. W. Weiler, M. L. Goldstein, and J.–L. Bougeret, 137–146, 2000.

Steinberg, J.–L., C. Lacombe, and S. Hoang, A new component of terrestrial radio emission observed from ISEE–3 and ISEE–1 in the Solar wind, *Geophys. Res. Lett.*, **15**, 176–179, 1988.

Steinberg, J.–L., S. Hoang, and J. M. Bosqued, Isotropic kilometric radiation: A new component of the Earth's radio emission, *Ann. Geophysicae*, **8**, 671–686, 1990.

Steinberg, J.–L., C. Lacombe, and S. Hoang, Sounding the flanks of the Earth's bow shock to -230 R_E: ISEE–3 observations of terrestrial radio sources down to 1.3 times the Solar wind plasma frequency, *J. Geophys. Res.*, **103**, 23565–23579, 1998.